Research Square

Preprints are preliminary reports that have not undergone peer review.
They should not be considered conclusive, used to inform clinical practice,
or referenced by the media as validated information.

Possibilities and limits of contrail avoidancethrough aircraft engine design and fuel selection

Julian Callard

callard@ist.rwth-aachen.de

RWTH Aachen University

Daniel Weintraub

RWTH Aachen University

Peter Jeschke

RWTH Aachen University

Research Article

Keywords: Contrails, Performance calculation, Engine cycle adaptation

Posted Date: June 9th, 2026

DOI: https://doi.org/10.21203/rs.3.rs-9554311/v1

License: This work is licensed under a Creative Commons Attribution 4.0 International License.
Read Full License

Additional Declarations: No competing interests reported.

Possibilities and limits of contrail avoidance through aircraft engine design and fuel selection

Julian Callard[1*], Daniel Weintraub[1] and Peter Jeschke[1]

[1*]Institute of Jet Propulsion and Turbomachinery, RWTH Aachen University, Templergraben 55, 52062, Aachen, Germany.

*Corresponding author(s). E-mail(s): callard@ist.rwth-aachen.de;
Contributing authors: weintraub@ist.rwth-aachen.de;
jeschke@ist.rwth-aachen.de;

Abstract

In this paper, we present a thermodynamic cycle-based analysis of the effect of aircraft engine design and fuel selection on contrail formation, which is evaluated using the Schmidt-Appleman criterion (SAC). Our goal is to examine the possibilities and limits of contrail avoidance to reduce the climate impact of aviation. We use the gas turbine performance software GasTurb to study geared-turbofan and open-rotor engine designs for contemporary short- to medium-range aircraft. The design parameters are overall pressure ratio, burner exit temperature, polytropic compressor and turbine efficiencies, and, for the geared-turbofan, also the design bypass ratio. We vary these parameters in wide ranges to cover all technically possible engine designs. We find that contrail formation at current cruise altitudes cannot be avoided with the examined contemporary and future engine cycles, unless the cycle design parameters are chosen in such a way that a significant specific fuel consumption penalty is incurred. In this case, the contrail formation altitude increases by less than 500 m. Future, more efficient engine cycles will increase contrail formation further. When using hydrogen as fuel instead of kerosene, contrails form at approximately 1.6 km lower altitudes. We thus find that it is practically impossible to avoid contrail formation, as predicted by the SAC, using the engine cycles and fuels examined in this paper. Operational contrail avoidance measures like cruise altitude adjustment or flying around ice-supersaturated atmospheric layers present themselves as more practicable.

Keywords: Contrails, Performance calculation, Engine cycle adaptation

Nomenclature

Roman letters

$\dot{m}_f$	Fuel flow	$\mathrm{kg\,s^{-1}}$
$\dot{Q}$	Heat flow	W
ALT	Altitude	m
$\mathrm{EI_{H2O}}$	Water emission index	-
FHV	Fuel heating value	$\mathrm{MJ\,kg^{-1}}$
SFC	Thrust specific fuel consumption	$\mathrm{g\,kN^{-1}\,s^{-1}}$
C_P	Specific heat capacity at constant pressure	$\mathrm{J\,kg^{-1}\,K^{-1}}$
C_V	Specific heat capacity at constant volume	$\mathrm{J\,kg^{-1}\,K^{-1}}$
F_N	Net thrust	kN
G	Mixing line slope	$\mathrm{Pa\,K^{-1}}$
m	Mass of air	kg
m_f	Fuel mass	$\mathrm{kg\,s^{-1}}$
P_D	Partial pressure of water vapour	Pa
P_s	Static pressure	Pa
Q	Heat	J
R_s	Specific gas constant	$\mathrm{J\,kg^{-1}\,K^{-1}}$
s	Distance	m
T	Total temperature	K
t	Time	s
T_s	Static temperature	K
U	Inner energy	J
V	Volume	$\mathrm{m^3}$
V_0	Aircraft velocity	$\mathrm{m\,s^{-1}}$
W	Work	J
W_V	Expansion work	J
W_{F_N}	Propulsive work	J

Greek letters

η_o	Overall engine efficiency	-
η_{pol}	Polytropic component efficiency	-
ε	Mass fraction	-

Subscripts

amb	Ambient
C	Critical
cruise	Cruise
fuel	Fuel

Abbreviations

$\mathrm{CO_2}$	Carbon dioxide
GTF	Geared-turbofan
ICAO	International civil aviation organization
nvPM	Non-volatile particulate matter
OR	Open-rotor
RF	Radiative forcing
SAC	Schmidt-Appleman criterion

VIGV Variable inlet guide vane
WET Water-enhanced turbofan

1 Introduction

Aircraft-induced contrails contribute significantly to the radiative forcing (RF) of aviation and thereby affect the climate. As part of the broader non-CO_2 effects, they are estimated to contribute at least as much – and possibly up to twice as much – to aviation's RF as CO_2 emissions [1–3]. They frequently form behind aircrafts in the upper troposphere and lower stratosphere [3]. Schmidt [4] and Appleman [5] developed the first thermodynamic theories on contrail formation. Schumann further developed these theories and validated them with flight tests [6, 7].
Contrails form when humid engine exhaust gases mix with dry ambient air. The mixing represents the necessary condition for contrail formation. If saturation with respect to liquid water is reached in the exhaust plume, water vapour from the combustion of fuel in the engine condenses on the condensation nuclei present in the exhaust stream. The nuclei are mainly made up of non-volatile emitted particulate matter (nvPM), like soot, and any ambient particles present [6]. The condensed water vapour forms liquid water droplets, which subsequently freeze to form contrails [3]. Reaching saturation constitutes the sufficient condition for contrail formation and is described by the Schmidt-Appleman criterion (SAC) formulated by Schumann [6].
In a dry atmosphere, the contrails usually dissipate quickly after forming. In atmospheric layers that are super-saturated with respect to ice, contrails do not dissipate and can remain in the atmosphere for longer. Such persistent contrails can begin to grow into contrail-induced cirrus clouds [6, 8] that reflect long-wavelength radiation back down to earth, thereby contributing the non-CO_2 RF [9]. The RF mechanisms of contrails and methods to reduce their climate impact are the subject of ongoing research [3, 8–13].
Contrail mitigation is comprised of technical and operational strategies. Operational strategies typically involve avoiding the ice-supersaturated areas by flight re-routing or level changes [14, 15]. The main difficulty faced by these approaches is the detection of and re-routing around ice-supersaturated atmospheric layers. This is avoided if contrails are prevented on a technical level in the engine itself.
In previous work, we investigated the potential for contrail mitigation by retrofitting existing engines using bypass and core nozzle areas, high- and low pressure turbine capacities, a handling bleed, and a high-pressure bleed [16]. The method we used relies on reducing the engine efficiency, which increases the exhaust gas temperature, thereby increasing the altitude where contrails just begin to form (critical altitude) [14, 16]. We found that the critical altitude can be increased by around 200 m for a contemporary geared-turbofan engine (GTF) at a cruise altitude of 10 km. This relatively small increase in critical altitude comes at the prohibitive cost of an increase in thrust specific fuel consumption (SFC) of 35 %, with significantly increased turbine temperatures [16]. The examined engine design and operating point changes did not prevent contrails from forming. Similarly, Haglind [17] found that utilizing variable inlet guide

vanes (VIGVs) in a turbofan engine increased the critical altitude of contrail formation by 300 m. This was accompanied by a 45 % increase in SFC. We therefore showed that retrofitting existing engines in the ways proposed above is no viable solution to reducing contrail formation during cruise.
Therefore, in this paper, we will take a step back and explore a wide design parameter range of future aero-engines to expand the take-away from our previous work.
The critical altitude of contrail formation also depends on the water emission index of the fuel used [6]. The water emission index divided by the heating value yields the energy-specific emission index. It is a measure of the water released per unit of energy released during fuel combustion. Alternative fuels, such as methane and hydrogen, with a higher energy-specific emission index produce contrails at lower altitudes compared to fuels with a lower index [14]. This effect can be counter-acted by the removal of water vapour from the exhaust gas [18–20].
In this work, we examine engines that use both hydrogen and kerosene as fuel to expand the study and include the effect of the emission index on the critical altitude. It should be noted here that the physical processes involved in contrail formation are highly complex and also depend on the properties and quantity of the exhaust particles and the dynamics of the nucleation of the ice [12, 13, 21–23].

2 Theory

In this section, we outline the thermodynamic theory to describe contrail formation. This brief summary is largely based on the work of Schumann [6]. We discussed some of this in our previous paper [16].
According to the SAC, contrails form if the exhaust plume-air mixture reaches saturation with respect to liquid water during the mixing process. As shown in Fig. 1, this mixing process starts out as a straight line in a partial pressure of water vapour vs. temperature diagram. The underlying assumptions are: ideal mixing, constant specific heat capacity, isobaric conditions, and that the partial pressure of water vapour is much smaller than the ambient pressure. This *mixing line* connects the engine exhaust conditions above and to the right of the diagram to the ambient conditions in the bottom left. Contrails can begin to form, when the mixing line crosses the water saturation curve. If a mixing line (shown in red in Fig 1) just touches the water saturation curve, contrails will just begin to form. Hence, contrails will form for a constant ambient humidity, if the ambient temperature T_{amb} is below a critical temperature T_C.

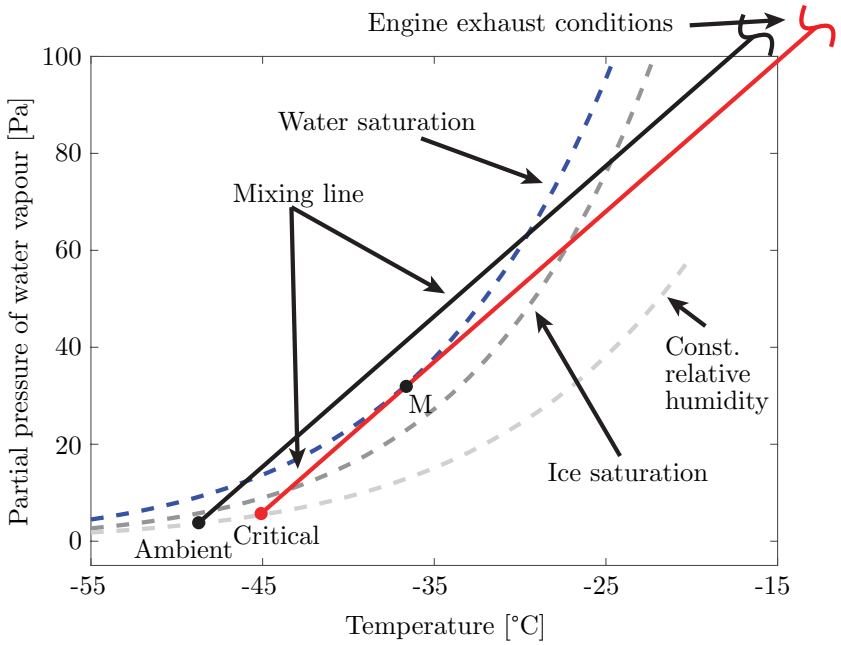


Fig. 1 Partial pressure of water vapour vs. temperature graph, derived from Schumann [7]. The red mixing line is chosen so that contrails just begin to form at point M for a critical ambient temperature at point C. Persistent contrails form if the ambient conditions are above the ice saturation line

According to Schumann, the gradient of the exhaust gas-ambient air mixing line can be expressed as

$$G = \frac{\Delta P_D}{\Delta T} = \frac{P_{\text{amb}} \text{EI}_{\text{H20}} C_P}{\varepsilon \, \text{FHV}(1 - \eta_o)} \tag{1}$$

where P_{amb} is the ambient pressure, EI_{H20} is the water emission index in $\text{kg}_{\text{water}}/\text{kg}_{\text{fuel}}$, C_P is the specific heat capacity. ε denotes the molar mass fraction of water to dry air, given as $\varepsilon = 0.622$. FHV is the fuel heating value and η_o the overall efficiency of the engine. η_o can be expressed as

$$\eta_o = \frac{F_N V_0}{\dot{m}_f \text{FHV}} \, , \tag{2}$$

with the net thrust F_N, aircraft velocity V_0, and fuel flow $\dot{m}_f$. Schumann [7] describes this as the η-effect and derives this relationship from an energy budget in a frame of reference fixed to the ambient air.

We intend to offer a new perspective on this, in the form of a set of assumptions that are compatible with the original derivation of the mixing line equation to make the η-effect more tangible. This set of assumptions, together with the analytical derivation of Eq. 1 from the first law of thermodynamics, is presented in the next section.

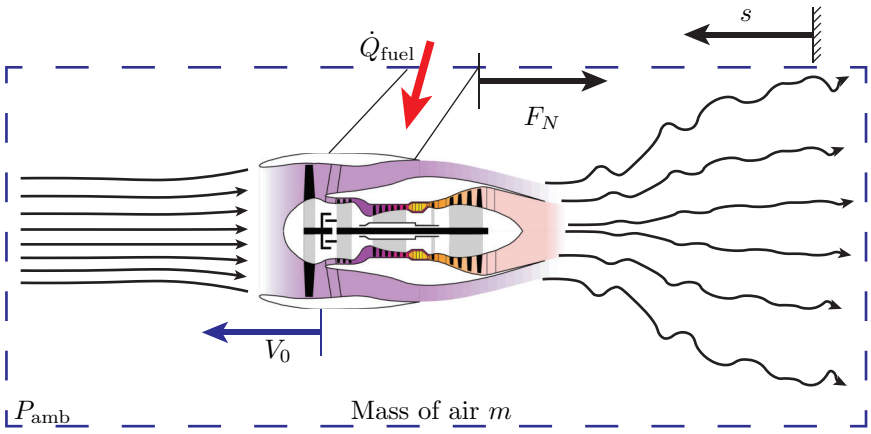


Fig. 2 Control volume for the derivation of the eta-effect by means of the first law of thermodynamics. The engine travels from right to left in direction s with velocity V_0, exerting the force F_N. The fuel heat flow $\dot{Q}_{\text{fuel}}$ is the only heat flow across the control volume boundary. Inside the volume is the mass of air m at ambient pressure P_{amb}

2.1 The slope of the mixing line G from the first law of thermodynamics

In this section, we present a set of assumptions together with a derivation for the slope of the mixing line, Eq. 1, from the first law of thermodynamics.
Fig. 2.1 shows the system boundaries around an aircraft engine in flight. It travels with velocity V_0 from right to left through a stationary control volume. The control volume heats up homogeneously, $\dot{Q}_{\text{fuel}}$ is the only heat flow across the system boundary, originating from the fuel flow to the engine. The engine exerts the thrust F_N through the pylon. Inside the control volume is the air mass m at ambient pressure P_{amb}. There is no mass flow across the system boundary, meaning that the control volume grows if the air inside heats up.
Then we can use the first law of thermodynamics

$$dU = dQ + dW. \tag{3}$$

The expansion work dW_V is defined by the volume change of the control system boundaries and the ambient pressure

$$dW_V = -P_{\text{amb}} dV\,. \tag{4}$$

The propulsive work dW_{F_N} performed by the engine is defined as the engine thrust times the distance covered

$$dW_{F_N} = -F_N ds\,. \tag{5}$$

The change in inner energy $dU = mC_V dT$, Eq. 3 then becomes

$$mC_V dT = dQ - P_{\text{amb}} dV - F_N ds. \tag{6}$$

During flight, the aircraft speed is known. To get from the distance covered to the aircraft speed, we differentiate with regard to time d/dt. Then we replace dV using the ideal gas equation

$$dV = \frac{mR_s}{P_{\text{amb}}} dT \,. \tag{7}$$

This yields Eq. 8.

$$\dot{Q}_{\text{fuel}} = F_N V_0 + m(C_V + R_s)\frac{dT}{dt} \,, \; with \; C_V + R_s = C_P \text{ and } V_0 = \frac{ds}{dt} \,. \tag{8}$$

The change in temperature inside the control volume goes towards $dT \to 0$, if the mass of air goes to infinity $m \to \infty$. Up to this part, the derivation represents the injection of energy into the atmosphere by the engine. We now need to derive the injection of water vapour from the burned fuel.
In the partial pressure of water vapour vs. temperature diagram, the slope of the mixing line under the assumptions outlined above, specifically the constant specific heat capacity, is defined as

$$G := \frac{dP_D}{dT} \,. \tag{9}$$

The change in the partial pressure of water vapour dP_D is

$$dP_D \approx \frac{P_{\text{amb}}}{\varepsilon} dx \,. \tag{10}$$

The change in water vapour content dx of the air depends on the water emission index of the used fuel and the mass of fuel burned during our timestep

$$dx = \text{EI}_{\text{H20}} \, d\left(\frac{m_f}{m}\right) \,. \tag{11}$$

To get from the mass of fuel burned to the mass flow of fuel, we again differentiate with regard to time

$$\frac{dp_D}{dt} \approx \frac{P_{\text{amb}} \, \text{EI}_{\text{H20}}}{\varepsilon \, m} \dot{m}_f \,, \quad \text{with } \dot{m}_f = \frac{dm_f}{dt} \,. \tag{12}$$

Inserting $\dot{Q}_{\text{fuel}} = \dot{m}_f \text{FHV}$ into Eq. 8 and re-arranging yields

$$\frac{dT}{dt} = \frac{-F_N V_0 + \dot{m}_f \text{FHV}}{m \, C_P} . \tag{13}$$

Then, dividing Eq. 12 by Eq 13, using Eq. 2, and multiplying with FHV/FHV finally yields the equation for the mixing line slope

$$G = \frac{P_{\text{amb}} \text{EI}_{\text{H20}} C_P}{\varepsilon \, \text{FHV}(1 - \eta_o)} . \tag{14}$$

2.2 Critical altitude

As stated in Sec. 2 the critical temperature is the temperature where, for a given ambient humidity, contrails will just begin to form. The mixing line slope G increases with engine efficiency, thus also increasing T_C. The critical temperature for a given engine configuration and cruise altitude can also be expressed as a critical altitude ALT_C, or change in critical altitude $\Delta\mathrm{ALT}_C$. The critical altitude is calculated with the ICAO-standard atmosphere equations [24] up to 11 km, as shown in Fig. 3.

$$\Delta\mathrm{ALT}_C = (T_{\mathrm{amb}} - T_C)\frac{1000\,\mathrm{m}}{6,5\,\mathrm{K}} \tag{15}$$

The difference in critical altitude can then be used to calculate the critical altitude for contrail formation

$$\mathrm{ALT}_C = \mathrm{ALT}_{\mathrm{cruise}} + \Delta\mathrm{ALT}_C \tag{16}$$

We employ the critical altitude as a metric that is used to evaluate the proposed thermodynamic cycles and fuel selection.

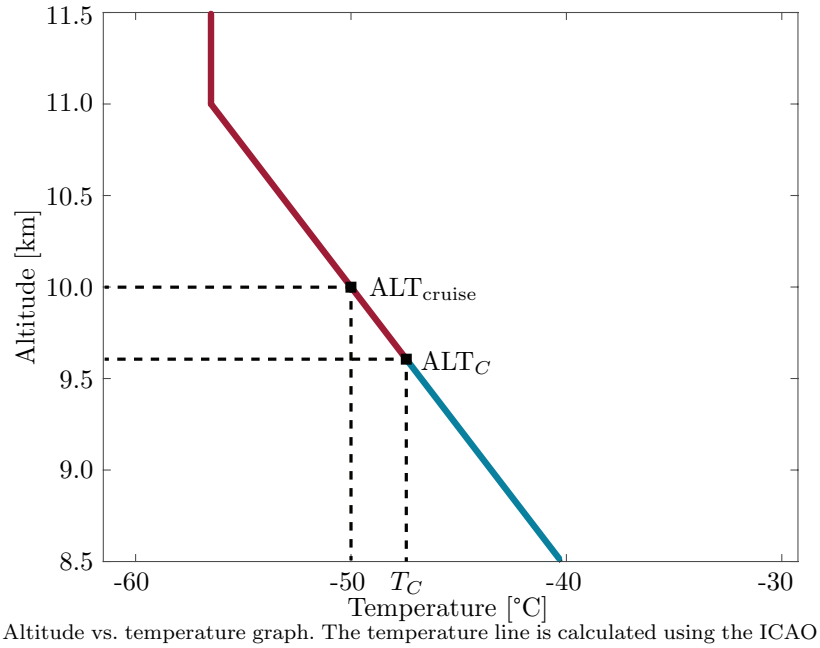


Fig. 3 Altitude vs. temperature graph. The temperature line is calculated using the ICAO standard atmosphere equations [24]. The red line indicates that contrails will form, the blue line that contrails will not form according to the Schmidt-Appleman criterion

Engine design parameter	Value
Design bypass ratio	10.7
Overall pressure ratio	35
Burner exit temperatur	1530 K
Polytropic efficiency	0.9

Table 1 Reference engine design parameters.

Engine design parameter	Lower limit	Upper limit
Design bypass ratio	1	15
Overall pressure ratio	30	70
Burner exit temperature	1450 K	1950 K
Polytropic efficiency	0.85	0.95

Table 2 GTF engine parameters.

Engine design parameter	Lower limit	Upper limit
Overall pressure ratio	15	60
Burner exit temperature	1450 K	1950 K
Polytropic efficiency	0.85	0.95

Table 3 OR engine parameters.

3 Methodology

Short- and medium range air traffic comprises 96 % of the total air traffic volume [25]. Therefore, the examined use-case is the short- to medium-range aircraft class (Airbus A320neo) in cruise flight. The operating point chosen is cruise flight, as contrails are typically formed during this flight phase. The reference engine is a modern GTF engine of the 120 kN thrust class. The reference engine design parameters are given in Tab. 1. The thrust requirement per engine is set at $F_N = 25$ kN, at a cruise altitude of $\mathrm{ALT}_{\mathrm{cruise}} = 10\,000$ m and $M_{\mathrm{cruise}} = 0.78$. The thrust requirement must be met by the examined engine cycles to maintain cruise speed and altitude. The batch job function is used in GasTurb [26–29] to vary the design parameters of the thermodynamic engine cycles of the future generic 2-spool GTF and 3-spool OR.
For the 2-spool GTF engine cycle, the design bypass ratio BPR, overall pressure ratio OPR, burner exit temperature T_4, and the compressors and turbines polytropic efficiencies η_{pol} are varied in between the limits given in Tab. 2. The OPR, T_4, and η_{pol} are varied according to Tab. 3 for the generic 3-spool OR configuration. The engine mass flow is used in an iteration to achieve the desired cruise thrust of $F_N = 25$ kN for each design parameter combination. The studies are then performed on each engine type for kerosene and hydrogen.
The Schmidt-Appleman criterion is implemented in MATLAB, with the values needed

for the calculation exported from GasTurb. MATLAB is also used for the post-processing of the data. The water and ice saturation vapour pressure curves are calculated according to the formulas presented by Sonntag [30].

4 Results

The study results are presented in this section, starting with the reference GTF configuration. Persistent contrails only form if the atmosphere is saturated with respect to ice. This is the case for relative humidity with respect to water of around 60 % for the studied temperature range. Therefore, the studies were evaluated at 60 % humidity to evaluate whether persistent contrails can form for the examined engine cycles. The critical altitude for each configuration was calculated according to Eq. 16.

4.1 Reference configuration

The mixing lines for kerosene and hydrogen fuel are shown in Fig. 4

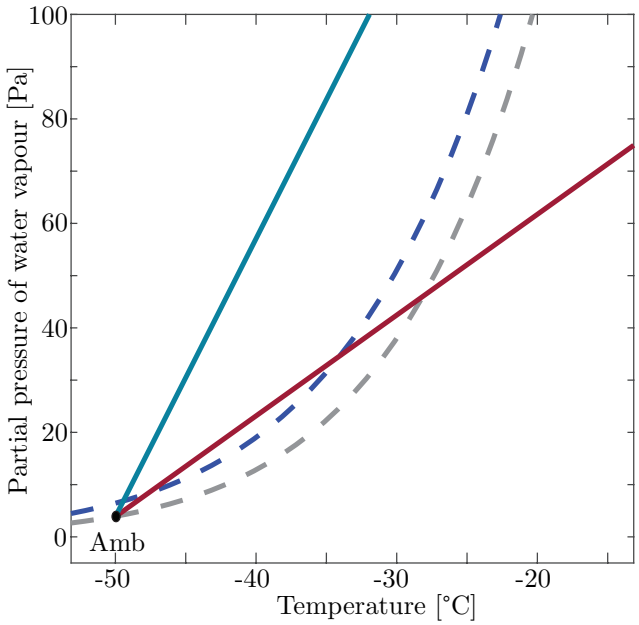


Fig. 4 Mixing lines for the reference configuration for kerosene (red) and hydrogen (blue) at the cruise conditions outlined in Sec. 3. Both fuel selections produce contrails

The water emission index of hydrogen is $EI_{H20,H2} = 9.21$ kg of water/kg of fuel, that of kerosene is $EI_{H20,K} = 1.24$ kg of water/kg of fuel. The cruise efficiency of the reference engine is $\eta_o = 0.37$. Using these values, the G-factor and critical altitude can be calculated. They are given in Tab. 4. Hydrogen fuel has a much higher water emission index compared to kerosene, which leads to contrail formation as low as 8 000

Fuel type	EI_{H20} [-]	FHV [MJ/kg]	η_o [-]	G [Pa/K]	ALT_{crit} [m]
Kerosene	1.24	43.12	0.37	1.93	9 627
Hydrogen	9.21	118.43	0.37	5.32	8 000

Table 4 Reference engine design parameters.

m for the reference configuration. Both configurations will produce contrails at cruise conditions and 60 % ambient humidity.

4.2 Geared-turbofan engine cycle

For the future GTF engine cycle, we first examined the design bypass ratio with varying humidity. The result for kerosene and $\eta_{pol} = 0.9$ is shown in Fig. 5. The critical temperature and therefore the critical altitude are influenced by the ambient humidity and the slope of the mixing line. With increasing ambient humidity, contrails are formed at higher ambient temperatures, resulting in a lower critical altitude.

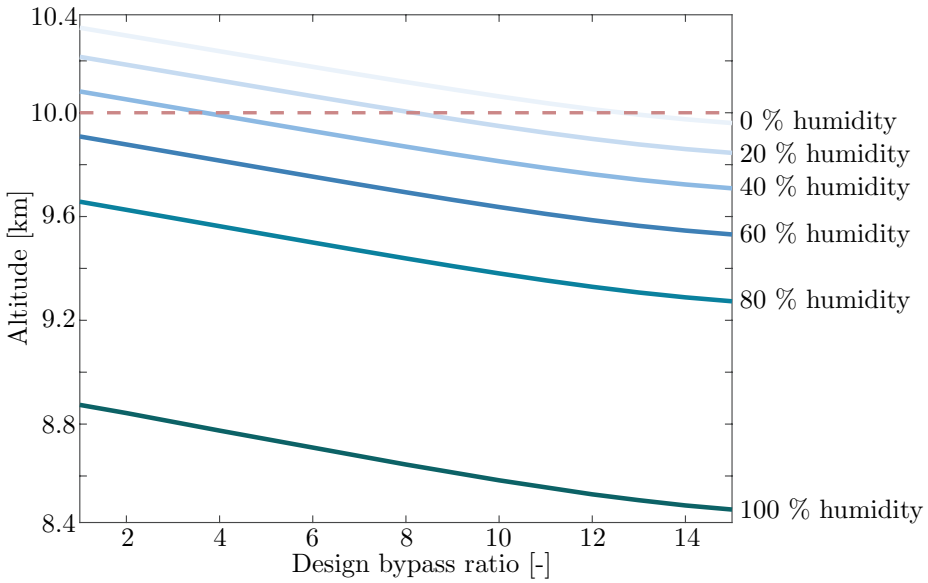


Fig. 5 Critical altitude as a function of the design bypass ratio and ambient humidity for the GTF engine cycle with kerosene. The red dotted line is the cruise altitude. For any part of a curve below this altitude contrails are formed according to the SAC

At 60 % ambient humidity, the critical altitude of a cycle with BPR = 1 is ALT_{crit} = 9.91 km. For BPR = 15, the critical altitude drops to 9.56 km. Greater ambient humidity further decreases the critical altitude. Increasing the bypass ratio increases the engine efficiency, which decreases the critical altitude.
Using hydrogen as a fuel further exacerbates this due to the increased water emission index, as shown in Fig. 6. The critical altitude decreases by around 1.6 km compared

to the kerosene configuration. For the BPR = 15 cycle at 60 % ambient humidity, the critical altitude is 7.86 km.

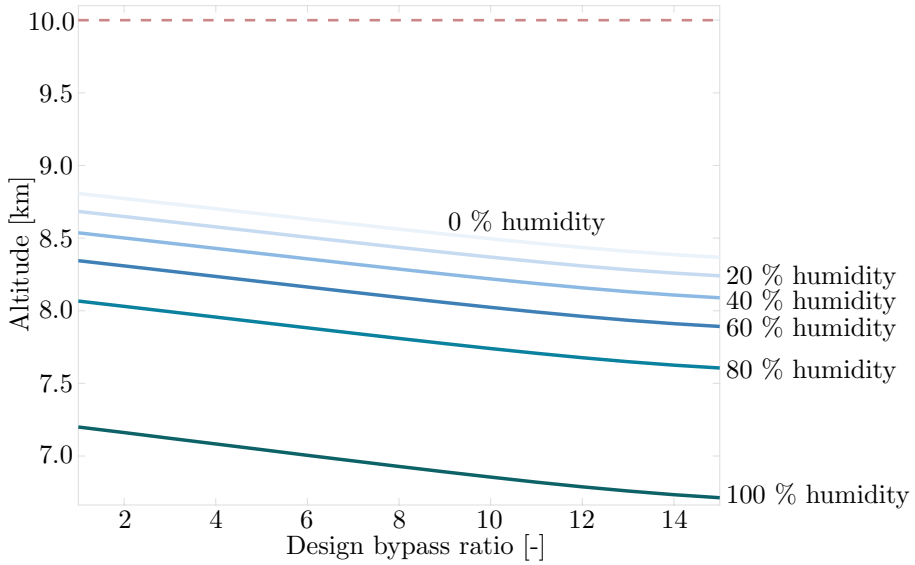


Fig. 6 Critical altitude as a function of the design bypass ratio and ambient humidity for the GTF engine cycle with hydrogen. The red dotted line is the cruise altitude. According to the SAC, the GTF cycles with hydrogen as a fuel will produce contrails at cruise altitude, regardless of ambient humidity

Fig. 7 shows the result of the variation of all the design parameters for a GTF with kerosene as the fuel, for a polytropic efficiency of $\eta_{\text{pol}} = 0.9$.

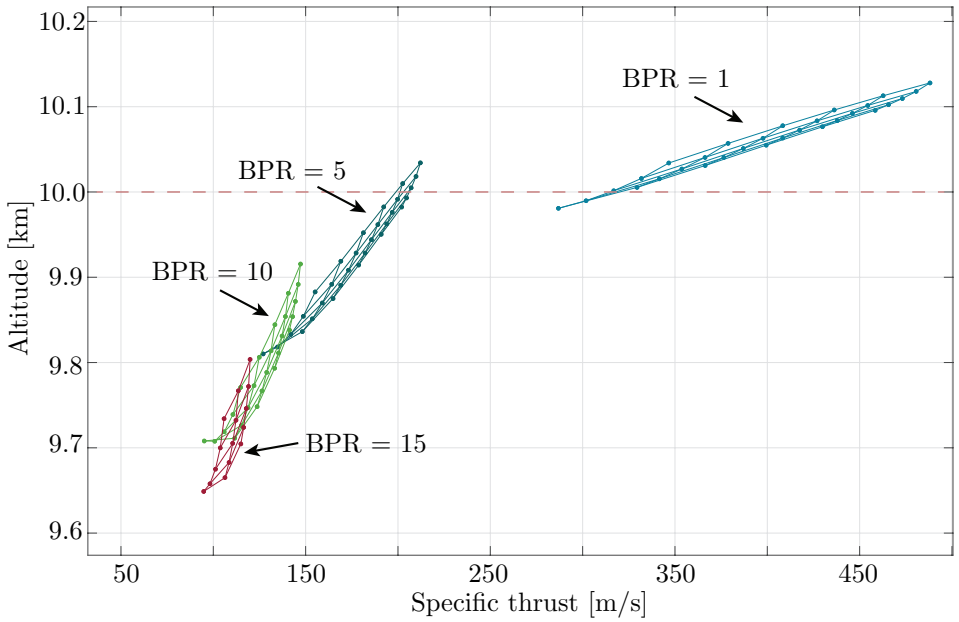


Fig. 7 Critical altitude as a function of design bypass ratio, burner exit temperature, and overall pressure ratio at 60 % ambient humidity vs. specific thrust. Specific thrust is chosen to make the surface plots clearly distinguishable. The design bypass ratio is the dominant design parameter with regards to critical altitude

Contrails are only avoided for engine cycles with BPR < 5. The bypass ratio has a greater influence on engine efficiency than the overall pressure ratio and the burner exit temperature. Most modern high bypass turbofan engines would produce contrails at the cruise conditions examined in this paper. The minimal critical altitude for the GTF engine cycles with kerosene is 9.65 km for BPR $= 15$, OPR $= 70$, and $T_4 = 1750$ K for an engine efficiency of $\eta_o = 0.396$. The highest critical altitude achieved is 10.12 km for BPR $= 1$, OPR $= 30$, and $T_4 = 1450$ K for $\eta_o = 0.168$. At high BPR the cycle cannot provide the thrust needed for T_4 lower than 1750 K.
Fig. 8 shows the result of the variation of all the design parameters for a GTF with hydrogen as the fuel, for a polytropic efficiency of $\eta_{\text{pol}} = 0.9$.

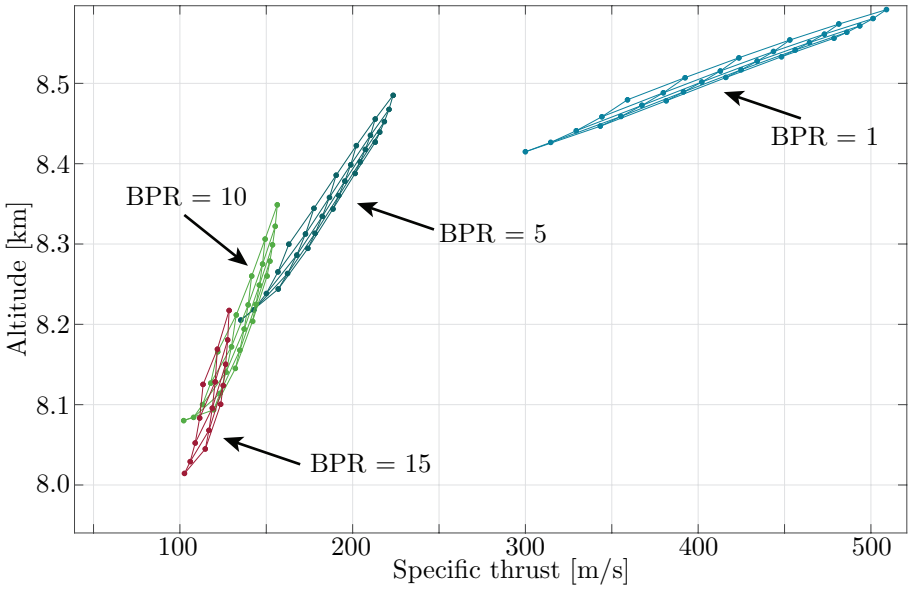


Fig. 8 Critical altitude as a function of design bypass ratio, burner exit temperature, and overall pressure ratio at 60 % ambient humidity vs. specific thrust for the hydrogen GTF engine cycle. Specific thrust is chosen to make the surface plots clearly distinguishable. The design bypass ratio is the dominant design parameter with regards to critical altitude

Unlike the results shown for the kerosene GTF cycle in Fig. 7, contrails cannot be avoided for any of the examined cycles using hydrogen as a fuel. The lowest critical altitude for $\eta_o = 0.411$ is $\mathrm{ALT}_{\mathrm{crit}} = 8.01$ km for BPR = 15, OPR = 70, and $T_4 = 1750$ K. The highest critical altitude is 8.59 km for $\eta_o = 0.166$ with the cycle design parameters BPR = 1, OPR = 30, and $T_4 = 1950$ K. The critical altitude for the hydrogen cycle is 1.6 km less on average roughly than for the kerosene cycle, when using the Schmidt-Appleman criterion.

4.3 Open-rotor engine cycle

The OR engine cycle parameters are varied according to Tab. 3. The critical altitude for the kerosene configuration is shown in Fig. 9 for $\eta_{\mathrm{pol}} = 0.9$. The highest critical altitude is 9.49 km for OPR = 15 and $T_4 = 1450$ K, and $\eta_o = 0.4$. Increasing the OPR decreases the critical altitude. Increasing T_4 also decreases the critical altitude for higher OPR values. The lowest critical altitude for the kerosene OR is $\mathrm{ALT}_{\mathrm{crit}} = 9.18$ km for OPR = 60 and $T_4 = 1950$ K at $\eta_o = 0.5$. According to the SAC, all kerosene OR engine configurations will produce contrails at the cruising altitude of 10 km.

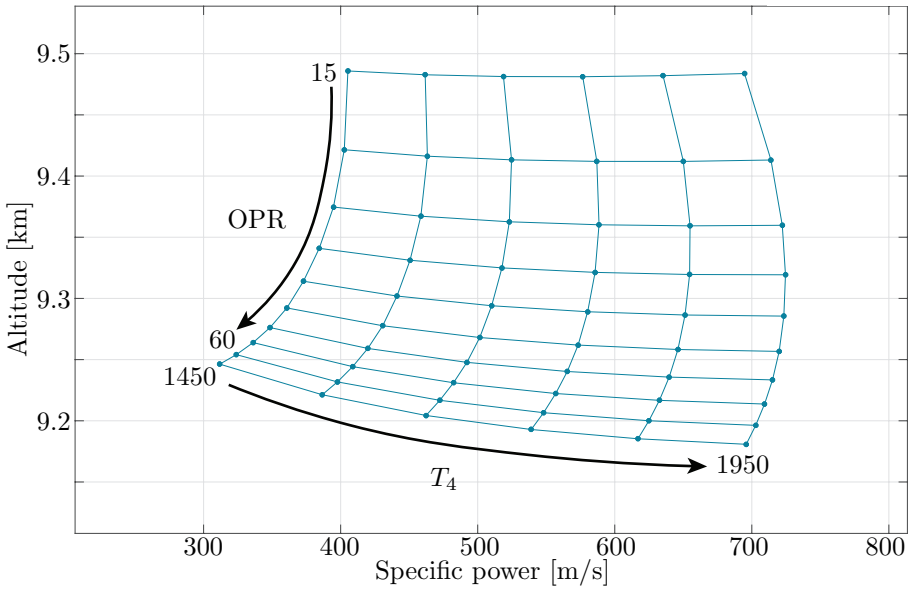


Fig. 9 Critical altitude as a function of the burner exit temperature and overall pressure ratio at 60 % ambient humidity vs. specific power for the kerosene OR engine cycle. Specific power is chosen to make the surface plots clearly distinguishable

Similarly to the GTF results, the critical altitude of the hydrogen OR engine configuration is around 1.6 km lower than that of the kerosene OR engine configuration. The results of the hydrogen OR are shown in Fig. 10 for $\eta_{\mathrm{pol}} = 0.9$.

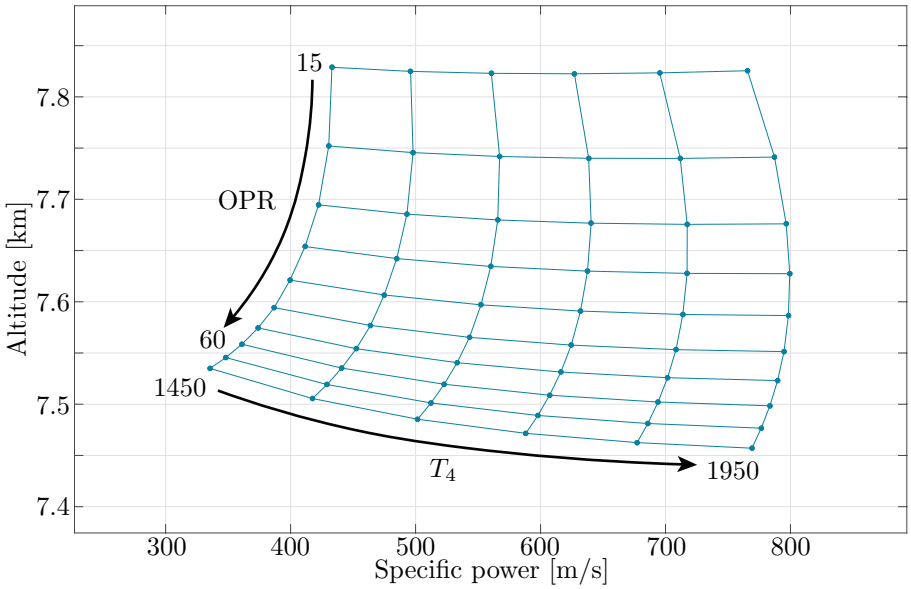


Fig. 10 Critical altitude as a function of the burner exit temperature and overall pressure ratio at 60 % ambient humidity vs. specific power for the hydrogen OR engine cycle. Specific power is chosen to make the surface plots clearly distinguishable

The highest critical altitude for the hydrogen OR is 7.82 km for OPR = 15 and T_4 = 1450 K at $\eta_o = 0.42$. The trends for OPR and T_4 are the same as for the kerosene OR configuration. The lowest critical altitude is 7.46 km for OPR = 60 and $T_4 = 1950$ K at $\eta_o = 0.52$. Again, all hydrogen OR engine configurations will produce contrails at 60 % ambient humidity at the cruise altitude of 10 km. To avoid contrails, the cruise altitude would have to be lowered below the critical altitude for the given engine configuration.

4.4 Overall results

The results can be summarised in a single critical altitude plot, as shown in Fig. 11. The altitude is on the y-axis. The x-axis is sectioned into three sections: reference configuration, GTF cycle adaptation, and OR cycle adaptation. The critical altitude is shown according to Tab. 4 for the reference configuration. The GTF and OR cycle adaptation critical altitude is shown as a range with blue hues indicating hydrogen as a fuel and gray/black indicating kerosene.

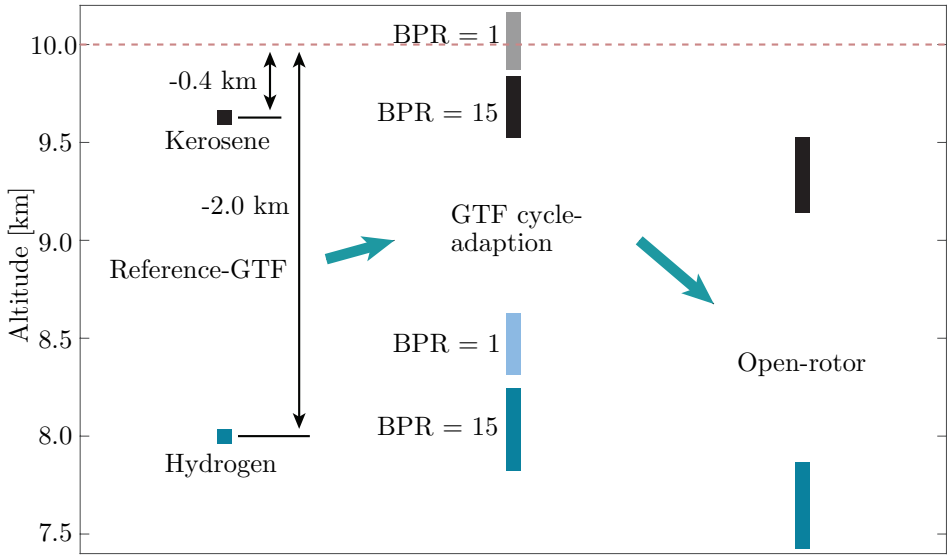


Fig. 11 This figure is a summary of the entire design space shown in Table 2 and 3 at 60 % ambient humidity and $\eta_{\text{pol}} = 0.9$. The critical altitude for each engine configuration is represented by the square (singular configuration) and rectangular (design space configurations) markers. The red dotted line is the cruise altitude. The critical altitude of the hydrogen cycles (blue hues) is roughly 1.6 km lower when compared to the kerosene cycles (black and grey hues)

The reference cruise altitude of 10 km is shown as the red dotted line. Any values of critical altitude below this line will produce contrails according to the SAC.
As discussed before, contrails are only avoided at cruise for inefficient GTF engine cycles with low BPR. All other cycles examined, including the reference configuration, will produce contrails at reference cruise altitude.

5 Discussion and conclusion

Engine cycle adaptations have the potential to increase the critical altitude at which contrails begin to form for a given engine configuration and cruise speed. Cycles that achieve an increase in critical altitude above the cruise altitude of 10 km examined in this paper are inefficient cycles with overall engine efficiencies below 25 %. The critical altitude of contrail formation at 60 % ambient humidity increased above 10 km for GTF engine cycles with a design bypass ratio of 1 and an overall engine efficiency of 16.8 %, when calculating the critical altitude with the Schmidt-Appleman criterion. The reference engine configuration and the other GTF and OR cycle adaptations all produce contrails at the reference cruise altitude. Therefore, preventing or avoiding persistent contrails is not possible with the engine configurations examined. All data on this are provided in full in the method and result sections of this paper.
Operational contrail prevention measures appear to be a more viable alternative to reduce the climate impact caused by the aviation industry. For kerosene, the cruise altitude has to be decreased by around 400 m to avoid persistent contrail formation for the reference configuration. For hydrogen, the altitude would have to be decreased by

around 2 km. For more efficient future engine configurations, the altitude correction would have to be 2.5 km for the most efficient OR engine cycles.
The calculations used in this paper can be used for future work to develop a robust, low-fidelity framework based on the Schmidt-Appleman criterion to predict whether contrails can form in flight. This information can then be used to calculate the level change needed to prevent persistent contrails from forming.

Appendix A Results for polytropic compressor and turbine efficiency of 0.95

This section contains the results for $\eta_{\mathrm{pol}} = 0.95$.

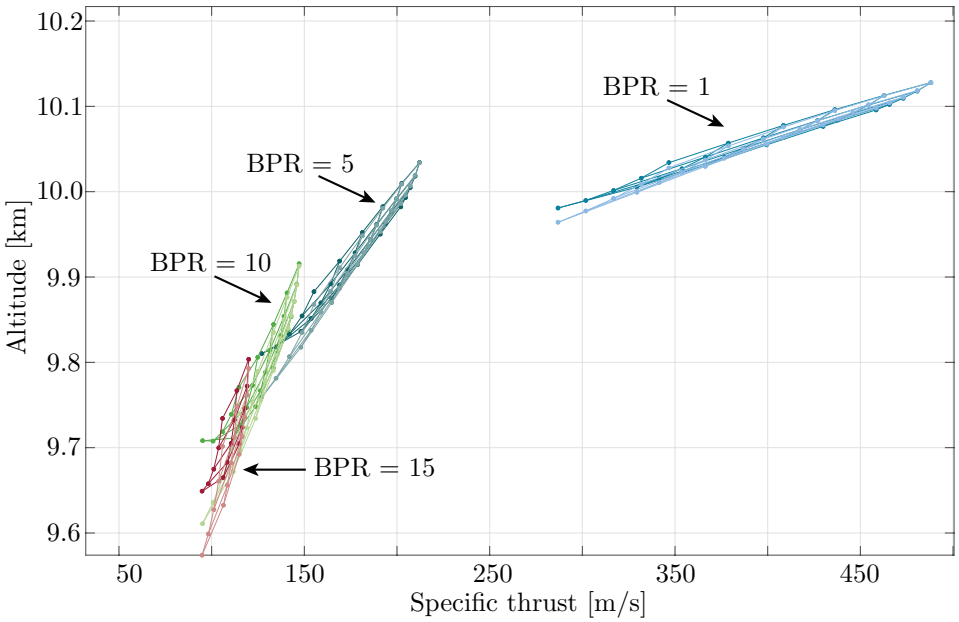


Fig. 12 Critical altitude as a function of design bypass ratio, burner exit temperature, overall pressure ratio, and polytropic compressor and turbine efficiency at 60 % ambient humidity vs. specific thrust for the kerosene GTF engine cycle. Specific thrust is chosen to make the surface plots clearly distinguishable. The design bypass ratio is the dominant design parameter with regards to critical altitude

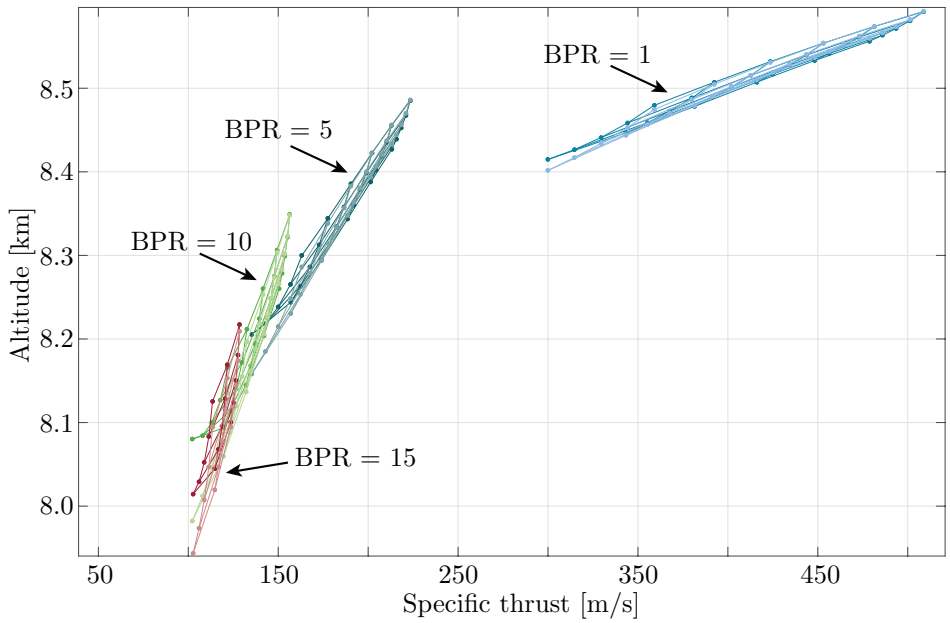


Fig. 13 Critical altitude as a function of design bypass ratio, burner exit temperature, overall pressure ratio, and polytropic compressor and turbine efficiency at 60 % ambient humidity vs. specific thrust for the hydrogen GTF engine cycle. Specific thrust is chosen to make the surface plots clearly distinguishable. The design bypass ratio is the dominant design parameter with regards to critical altitude

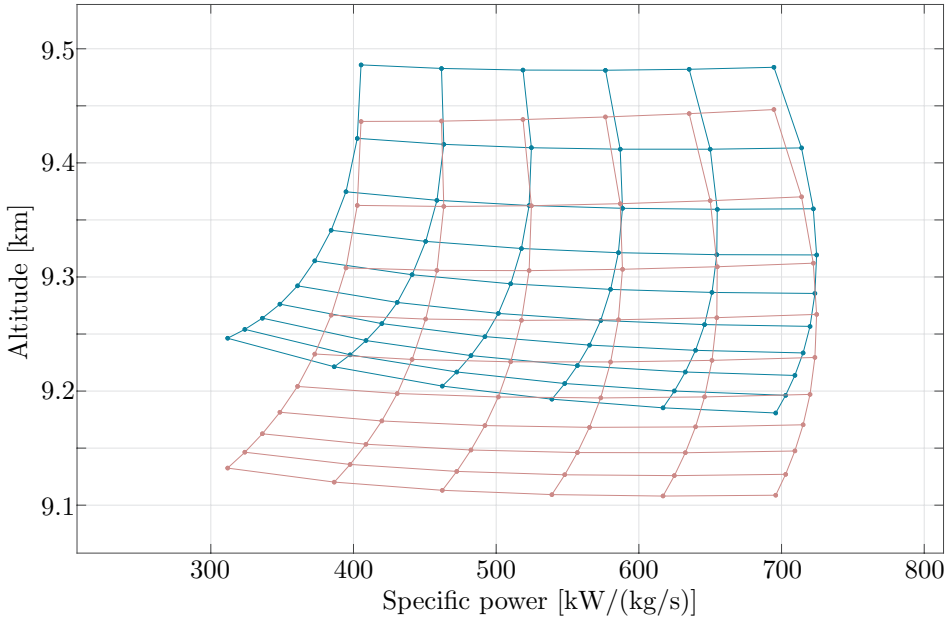


Fig. 14 Critical altitude as a function of the burner exit temperature, overall pressure ratio, and polytropic compressor and turbine efficiency at 60 % ambient humidity vs. specific power for the kerosene OR engine cycle. Specific power is chosen to make the surface plots clearly distinguishable

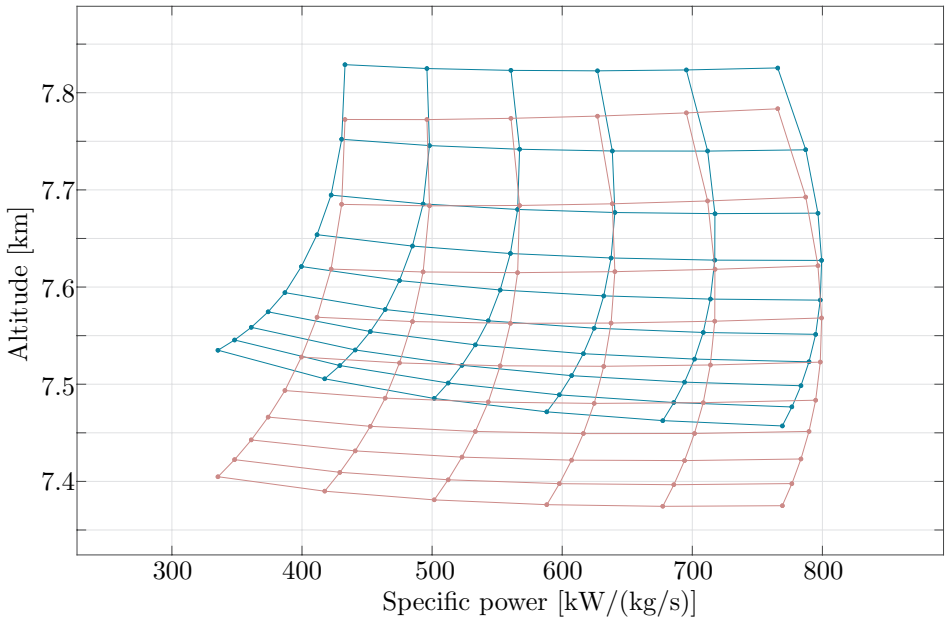


Fig. 15 Critical altitude as a function of the burner exit temperature, overall pressure ratio, and polytropic compressor and turbine efficiency at 60 % ambient humidity vs. specific power for the hydrogen OR engine cycle. Specific power is chosen to make the surface plots clearly distinguishable

References

[1] Lee, D.S., Fahey, D.W., Skowron, A., Allen, M.R., Burkhardt, U., Chen, Q., Doherty, S.J., Freeman, S., Forster, P.M., Fuglestvedt, J., Gettelman, A., León, R.R., Lim, L.L., Lund, M.T., Millar, R.J., Owen, B., Penner, J.E., Pitari, G., Prather, M.J., Sausen, R., Wilcox, L.J.: The contribution of global aviation to anthropogenic climate forcing for 2000 to 2018. Atmospheric Environment **244**, 117834 (2021) https://doi.org/10.1016/j.atmosenv.2020.117834

[2] Burkhardt, U., Kärcher, B.: Global radiative forcing from contrail cirrus. Nature Climate Change **1**, 54–58 (2011) https://doi.org/Ulrike

[3] Kärcher, B.: Formation and radiative forcing of contrail cirrus. Nature Communications **9**(1), 1824 (2018) https://doi.org/10.1038/s41467-018-04068-0

[4] Schmidt, E.: Die entstehung von eisnebel aus den auspuffgasen von flugmotoren. Schiften der Deutschen Akademie der Luftfahrtforschung **44**(5) (1941)

[5] Appleman, H.: The formation of exhaust condensation trails by jet aircraft. Bulletin American Meteorological Society **34**(1), 14–20 (1953)

[6] Schumann, U.: On conditions for contrail formation from aircraft exhausts. Meteorologische Zeitschrift **5**(1), 4–23 (1996)

[7] Schumann, U., Busen, R., Plohr, M.: Experimental test of the influence of propulsion efficiency on contrail formation. Journal of Aircraft **37**(6), 1083–1087 (2000)

[8] Schumann, U.: Formation, properties and climatic effects of contrails. Comptes Rendus Physique **6**, 549–565 (2005). Accessed 21.08.2024

[9] Meerkötter, R., Schumann, U., Doelling, D.R., Minnis, P., Nakajima, T., Tsushima, Y.: Radiative forcing by contrails. Annales Geophysicae **17**(8), 1080–1094 (1999) https://doi.org/10.1007/s00585-999-1080-7

[10] van de Hulst, H.C.: Light Scattering by Small Particles. Dover Publications, Inc., New York (1957)

[11] Minnis, P., Palikonda, R., Walter, B.J., Ayers, J.K., Mannstein, H.: Contrail properties over the eastern north pacific from avhrr data. Meteorologische Zeitschrift **14**, 515–523 (2005) https://doi.org/Bryan

[12] Ramsay, J., Tristanto, I., Shahpar, S., John, A.: Assessing the impact of turbofan engine design on aircraft contrail properties. ASME Journal of Engineering for Gas Turbines and Power **148** (2026)

[13] Narciso, M., Sousa, J.M.M.: Influence of sustainable aviation fuels on the formation of contrails and their properties. Energies **14**(17), 5557 (2021) https:

//doi.org/10.3390/en14175557

[14] Gierens, K., Lim, L., Eleftheratos, K.: A review of various strategies for contrail avoidance. The Open Atmospheric Science Journal **2**, 1–7 (2008). Accessed 21.08.2024

[15] Teoh, R., Schumann, U., Majumdar, A., Stettler, M.E.J.: Mitigating the climate forcing of aircraft contrails by small-scale diversions and technology adoption. Environmental science & technology **54**(5), 2941–2950 (2020) https://doi.org/10.1021/acs.est.9b05608

[16] Callard, J., Klumpp, C., Weintraub, D., Henninger, S., Jeschke, P.: Reducing contrail formation by engine design and operating point adaptation of aircraft engines. CEAS Aeronautical Journal (2025) https://doi.org/10.1007/s13272-025-00887-2

[17] Haglind, F.: Potential of lowering the contrail formation of aircraft exhausts by engine re-design. Aerospace Science and Technology **12**(6), 490–497 (2008) https://doi.org/10.1016/j.ast.2007.12.001

[18] Noppel, F., Singh, R., Taylor, M.: Novel engine concept to suppress contrail and cirrus cloud formation. Precedings of the TAC-Conference, 221–240 (2006)

[19] Pouzolz, R., Schmitz, O., Klingels, H.: Evaluation of the climate impact reduction potential of the water-enhanced turbofan (wet) concept. Aerospace **8**(3), 59 (2021) https://doi.org/10.3390/aerospace8030059

[20] Gao, X., Isoldi, A., Nalianda, D., Nikolaidis, T.: Water extraction in aero gas turbines for contrail mitigation. The Aeronautical Journal **128**(1325), 1344–1361 (2024) https://doi.org/10.1017/aer.2024.22

[21] Burkhardt, U., Bock, L., Bier, A.: Mitigating the contrail cirrus climate impact by reducing aircraft soot number emissions. npj Climate and Atmospheric Science **1**(1) (2018) https://doi.org/10.1038/s41612-018-0046-4

[22] Voigt, C., Kleine, J., Sauer, D., Moore, R.H., Bräuer, T., Le Clercq, P., Kaufmann, S., Scheibe, M., Jurkat-Witschas, T., Aigner, M., Bauder, U., Boose, Y., Borrmann, S., Crosbie, E., Diskin, G.S., DiGangi, J., Hahn, V., Heckl, C., Huber, F., Nowak, J.B., Rapp, M., Rauch, B., Robinson, C., Schripp, T., Shook, M., Winstead, E., Ziemba, L., Schlager, H., Anderson, B.E.: Cleaner burning aviation fuels can reduce contrail cloudiness. Communications Earth & Environment **2**(1) (2021) https://doi.org/10.1038/s43247-021-00174-y

[23] Williams, V.: The engineering options for mitigating the climate impacts of aviation. Philosophical transactions. Series A, Mathematical, physical, and engineering sciences **365**(1861), 3047–3059 (2007) https://doi.org/10.1098/rsta.2007.0012

[24] ICAO: Manual of the ICAO Standard Atmosphere: extended to 80 km (262 500 feet) - DOC7488/3 (1993)

[25] Wilkerson, J.T., Jacobson, M.Z., Malwitz, A., Balasubramanian, S., Wayson, R., Fleming, G., Naiman, A.D., Lele, S.K.: Analysis of emission data from global commercial aviation: 2004 and 2006. Atmos. Chem. Phys. **10**, 6391–6408 (2010)

[26] GasTurb GmbH: GasTurb 14. GasTurb GmbH (2025)

[27] Kurzke, J., Halliwell, I., Hill, R.: Propulsion and Power. Springer Nature Switzerland, Cham (2025). https://doi.org/10.1007/978-3-031-65026-0

[28] Saravanamuttoo, H.I.H., Rogers, G.F.C., Cohen, H.: Gas Turbine Theory, 12 edn. Dorling Kindersley, India (2013)

[29] Mattingly, J.D.: Elements of Gas Turbine Propulsion. Tata McGraw, New Delhi (2005)

[30] Sonntag, D.: Fortschritte in der hygrometrie. Meteorologische Zeitschrift **3**(2), 51–66 (1994) https://doi.org/10.1127/metz/3/1994/51